

STELLAR NUCLEOSYNTHESIS IN THE HYADES OPEN CLUSTER¹

Simon C. Schuler^{2,4}, Jeremy R. King³, AND Lih-Sin The³

ABSTRACT

We report a comprehensive light element (Li, C, N, O, Na, Mg, and Al) abundance analysis of three solar-type main sequence (MS) dwarfs and three red giant branch (RGB) clump stars in the Hyades open cluster using high-resolution and high signal-to-noise spectroscopy. The abundances have been derived in a self-consistent fashion, and for each group (MS or RGB), the CNO abundances are found to be in excellent star-to-star agreement. Using the dwarfs to infer the initial composition of the giants, the combined abundance patterns confirm that the giants have undergone the first dredge-up and that material processed by the CN cycle has been mixed to the surface layers. The observed abundances are compared to predictions of a standard stellar model based on the Clemson-American University of Beirut (CAUB) stellar evolution code. The model reproduces the observed evolution of the N and O abundances, as well as the previously derived $^{12}\text{C}/^{13}\text{C}$ ratio, but it fails to predict by a factor of 1.5 the observed level of ^{12}C depletion. A similar discord appears to exist in previously reported observed and modeled C abundances of giants in the Galactic disk. Random uncertainties in the mean abundances and uncertainties related to possible systematic errors in the Hyades dwarf and giant parameter scales cannot account for the discrepancy in the observed and modeled abundances. Li abundances are derived to determine if non-canonical extra mixing, like that seen in low-mass metal-poor giants, has occurred in the Hyades giants. The

¹Based on data taken with the Harlan J. Smith 2.7-m telescope at The McDonald Observatory of the University of Texas at Austin.

²National Optical Astronomy Observatory, 950 North Cherry Avenue, Tucson, AZ, 85719; sschuler@noao.edu

³Department of Physics and Astronomy, Clemson University, 118 Kinard Laboratory, Clemson, SC, 29634; jking2@ces.clemson.edu, tlihsin@clemson.edu

⁴Leo Goldberg Fellow

Li abundance of the giant γ Tau is in good accord with the predicted level of surface Li dilution, but a ~ 0.35 dex spread in the giant Li abundances is found and cannot be explained by the stellar model. Possible sources of the spread are discussed; however, it is apparent that the differential mechanism responsible for the Li dispersion must be unrelated to the uniformly low ^{12}C abundances of the giants. Na, Mg, and Al abundances are derived as an additional test of our stellar model. All three elements are found to be overabundant by 0.2 – 0.5 dex in the giants relative to the dwarfs. Such large enhancements of these elements are not predicted by the stellar model, and non-LTE effects significantly larger (and, in some cases, of opposite sign) than those implied by extant literature calculations are the most likely cause.

Subject headings: open clusters and associations: individual(Hyades) — nuclear reactions, nucleosynthesis, abundances — stars: abundances — stars: atmospheres — stars: interiors — stars: evolution

1. INTRODUCTION

The CN cycle is the dominant energy source in the H burning cores of main sequence (MS) stars more massive than the Sun. The cycle effectively converts four protons into a ^4He nucleus using ^{12}C , ^{13}C , ^{14}N , and ^{15}N as catalysts for the reactions. If O is present, the ON cycle can inject ^{14}N into the CN cycle at the expense of ^{16}O . The combined CNO bi-cycle produces no net loss of CNO nuclei, but their relative abundances are altered due to their different lifetimes against proton capture. The slowest reaction in the cycle, $^{14}\text{N}(p, \gamma)^{15}\text{O}$, creates a bottleneck, and by the time the reactions achieve a steady state, the abundance of ^{12}C and the related $^{12}\text{C}/^{13}\text{C}$ ratio have been reduced, and the abundance of ^{14}N has been increased.

Prior to the onset of core He burning, the convective envelope extends from the stellar surface down to the inner layers, reaching depths where the CN cycle had been previously active (Iben 1964). Known as the first dredge-up, the extended convective envelope chemically homogenizes the outer and inner layers down to an interior mass of about $0.5 M_{\odot}$ (depending on the mass and metallicity of the progenitor star), and products of the core nuclear processes once shrouded by the star’s optically thick layers are now brought to the surface where they can be observed. No additional alteration of the surface composition is expected until the star evolves off of the red giant branch (RGB).

Many high-resolution spectroscopic studies have targeted CNO and other light elements

such as Li, Na, Mg, and Al (the abundances of which may be affected by core nuclear processes and the first dredge-up) in order to verify the general scenario outlined above and to test the quantitative predictions of stellar evolution models. Observed CNO abundance patterns, and $^{12}\text{C}/^{13}\text{C}$ ratios, of near-solar metallicity giants in general have been found to be in good agreement with standard stellar evolution models (e.g., Lambert & Ries 1981; Luck & Heiter 2007), but there are exceptions. Gilroy (1989) found $^{12}\text{C}/^{13}\text{C}$ ratios of 15 ± 3 for some open cluster giants, well below typical predicted values of about 23 – 25 (e.g., Salaris et al. 2002). Standard models are those in which mixing is done by convection only; non-canonical mixing mechanisms such as rotationally-induced mixing are not included.

Standard models are also unable to reproduce the light element abundances of low-mass ($M \lesssim 2.5 M_{\odot}$) metal-poor giants brighter than the RGB bump. These giants have $^{12}\text{C}/^{13}\text{C}$ ratios that are generally below 10 and often reach near the equilibrium value of ~ 3.5 ; they also have depleted ^{12}C and enhanced ^{14}N abundances relative to giants at the bump and essentially no Li (e.g., Gratton et al. 2000; Shetrone 2003). The observed abundance patterns are believed to be the result of an extra mixing episode subsequent to the RGB bump, and shear instabilities and thermohaline mixing have been shown to be promising non-canonical mixing mechanisms that can account for the observations (e.g., Denissenkov et al. 2006; Charbonnel & Zahn 2007).

Despite overall good agreement between observations and stellar evolution models, it is clear that standard models are incomplete, and light element abundance analyses of giants with different masses and metallicities will continue to provide valuable empirical constraints for future theoretical efforts. The chemical homogeneity of open clusters make them excellent laboratories for this purpose. Open cluster dwarf abundances can be used as a proxy for the initial metallicity of giants in the same cluster, allowing the surface abundance evolution resulting from the first dredge-up to be empirically quantified. The light element abundances of open cluster giants have been derived by numerous previous groups (e.g., Lambert & Ries 1977, 1981; Brown 1985; Gilroy 1989; Tautvaišienė et al. 2000), but none have simultaneously determined dwarf and giant abundances from the same data set. Pasquini et al. (2004) performed a detailed chemical analysis of 22 stars, ranging from MS dwarfs to post-RGB clump giants, in the open cluster IC 4651. Li, Na, Mg, and Al were included in the analysis, but CNO were not.

We report here the first comprehensive light-element abundance analysis of both MS dwarfs and RGB clump giants in the Hyades open cluster carried-out in a self-consistent fashion. Abundances of Li, C, N, Na, Mg, and Al are newly derived from a homogeneous set of high-resolution echelle spectra, and combined with O abundances previously derived from the same spectra (Schuler et al. 2006a), we conduct a critical comparison between the

observed light-element abundances and the predictions of a standard stellar evolution model tailored to the Hyades giants.

2. STELLAR EVOLUTION MODEL

We have employed the Clemson-American University of Beirut (CAUB) stellar evolution code (The et al. 2000; El Eid et al. 2004; The et al. 2007), a 1D implicit hydrodynamical Lagrangian code, to model the surface compositions of the Hyades giants. In its general form, the code evolves a star by first solving the stellar structure equations, then by performing the nuclear burning for the given time step, and finally by diffusively mixing the nuclear species present in the convective zones. However, the code has been improved recently so that it can carry out simultaneously the nuclear burning and mixing stages. This allows the inclusion of the Cameron-Fowler mechanism, the nucleosynthesis and mixing timescales for which are quite similar, and its possible effects on the Li surface abundance. We find that the nucleosynthesis results of both recipes are in good agreement up to the end of core He burning; for example, no significant difference in the ${}^7\text{Li}$ surface abundance before and after the first dredge-up is seen between the two calculations.

The thermonuclear reaction rates included in the CAUB code are from the NACRE collaboration (Angulo et al. 1999) and are complemented by the NonSmoker compilation of Rauscher & Thielemann (2000). The nuclear data are taken from the study of Audi & Wapstra (1995). For the important reaction ${}^{12}\text{C}(\alpha,\gamma){}^{16}\text{O}$, we adopt the rate given by Kunz et al. (2002), who have reduced considerably the uncertainties in the relevant cross section at stellar temperatures. The code uses an electron-positron equation of state (EOS) based on table interpolation of the Helmholtz Free energy of Timmes & Swesty (2000). The EOS solves the Saha equation for partially ionized matter, and it is accurate for any degree of degeneracy and relativistic matter covering $10^{-12} \leq \rho \leq 10^{15} \text{ g cm}^{-3}$ and $10^3 \leq T \leq 10^{13} \text{ K}$. EOS_2005 Rosseland mean opacities from Livermore (Iglesias & Rogers 1996) have been used for the H-rich and exhausted H compositions. For the stellar layers with temperatures lower than $\sim 6000 \text{ K}$, the Rosseland mean opacities calculated by Ferguson et al. (2005) are used. The code makes use of the Schwarzschild criterion of convection in determining the convective zones in the stellar model; neither overshooting nor semiconvection is included in the calculations. A mixing length parameter $\alpha = 2.0$ ($l = \alpha H_p$, where l is the convective scale length and H_p is the local pressure scale height) has been adopted. Because mass loss is expected to be minor in low mass stars, it is not included in the evolution of the model.

The stellar model, which is characterized by a mass of $2.5 M_{\odot}$ and an initial metallicity of $Z = 0.025$ ($[\text{m}/\text{H}] \simeq +0.10^5$), is an updated version of the one used in our previous Hyades

study, where the mass and metallicity of the model are discussed (Schuler et al. 2006a). Throughout this paper we adopt the Hyades metallicity (i.e., $[\text{Fe}/\text{H}]$) of Paulson et al. (2003, $[\text{Fe}/\text{H}] = +0.13$), and the metallicity of the stellar model was chosen to closely match this value. The model begins at the zero main sequence phase with $\log T_{\text{eff}} = 4.027$, $\log(L/L_{\odot}) = 1.632$, central temperature $T_{\text{C}} = 2.28 \times 10^7$ K, and central density $\rho_{\text{C}} = 4.687 \times 10^1 \text{ gcm}^{-3}$. At this time, the H convective core is at its maximum mass, $0.436 M_{\odot}$. The model reaches the end of the core H burning phase when its central nuclear energy generation is at a minimum, which occurs after an evolution time of 5.121×10^8 yr. At this stage of the calculation, the star is characterized by a $\log T_{\text{eff}} = 3.921$, $\log(L/L_{\odot}) = 1.824$, $T_{\text{C}} = 2.57 \times 10^7$ K, $\rho_{\text{C}} = 7.678 \times 10^2 \text{ gcm}^{-3}$, and a central ${}^4\text{He}$ mass fraction $X({}^4\text{He}) = 0.9786$. Up until this point, the photospheric elemental mass fractions of the MS star have not been altered from their initial values.

After the end of the core H burning stage approximately 1.275×10^7 yr later, the first dredge-up starts to develop and reaches a maximum depth at an interior radius of $M_{\text{r}} = 0.338 M_{\odot}$, before the He convective core begins to develop. During the inward progression of the convective envelope (which lasts only for $\sim 1.51 \times 10^7$ yr), the elemental surface mass fractions show some transformation due to the mixing of envelope material with the products of the core H burning. After the first dredge-up, no additional alteration of the surface abundances is seen until the onset of the third dredge-up (during shell He burning). During core He burning, the bottom of the convective envelope retracts outward to an interior radius of $M_{\text{r}} = 1.480 M_{\odot}$. The convective He core grows up to a maximum of $0.242 M_{\odot}$, with He burning in the core lasting for $\sim 2.82 \times 10^8$ yr. Observationally, the Hyades giants are currently residing at the cluster RGB clump (de Bruijne et al. 2001), and are thus in their core He-burning stages.

2.1. Evolution of Surface Abundances

Figure 1 shows the composition profiles after the end of core H burning, before the first dredge-up of our $2.5 M_{\odot}$ stellar model; Figure 2 shows the composition profiles after the first dredge-up but before core He burning ignites. The first dredge-up lasts a very short time ($\sim 1.5 \times 10^7$ yrs) relative to the duration of core H (5.12×10^8 yrs) or core He burning ($\sim 2.8 \times 10^8$ yrs). However, many isotopic surface abundances change dramatically during the dredge-up process.

Fig.1
Fig.2

⁵Throughout this paper we use the standard bracket notation to denote stellar abundances given relative to solar values, e.g., $[\text{m}/\text{H}] = \log[N(\text{m})/N(\text{H})]_{*} - \log[N(\text{m})/N(\text{H})]_{\odot}$ on a scale where $\log N(\text{H}) = 12.0$.

Comparing the energy generation rate of the proton-proton (p-p) chains with that of the CNO bi-cycle we find that a star with a mass larger than $\sim 1.3 M_{\odot}$ or having a central temperature greater than $\sim 1.7 \times 10^7$ K has its energy generation dominated by the CNO bi-cycle (Arnett 1996). To understand the features of the composition profiles in Figure 1, we look at the properties of the p-p chains, CNO bi-cycle (Clayton 1968), and the NeNa and MgAl cycles (Rolfs & Rodney 1988). Examining the profiles from the surface inward, the temperature in the star increases, and we notice the first observable consequence of the p-p chains, i.e., the destruction of ${}^7\text{Li}$ through ${}^7\text{Li}(p,\alpha){}^4\text{He}$ reaction ($T \gtrsim 3.8 \times 10^6$ K). Somewhat further inward, we encounter the location where most of the ${}^{10}\text{B}$ has been destroyed through the ${}^{10}\text{B}(p,\alpha){}^7\text{Li}$ reaction ($T \gtrsim 6.0 \times 10^6$ K). During the early evolution of H burning, the ${}^7\text{Li}$ and ${}^{10}\text{B}$ profiles trail each other as their steep destruction profiles move further outward. Furthermore, due to their steep profiles and their proximity in the stellar atmosphere, the mass-thickness ratio of the ${}^7\text{Li}$ and ${}^{10}\text{B}$ profiles before the first dredge-up can be estimated by the ${}^7\text{Li}$ and ${}^{10}\text{B}$ abundance ratios in the dwarf and giant stars. Further inward, we find another product of the p-p chains, ${}^3\text{He}$, that was predominantly produced through ${}^2\text{D}(p,\gamma){}^3\text{He}$ ($T \gtrsim 7.7 \times 10^6$ K). However, at higher temperatures ($T \gtrsim 13.5 \times 10^6$ K), ${}^3\text{He}$ is predominantly self-destructed through ${}^3\text{He}({}^3\text{He},2p){}^4\text{He}$ reactions.

With respect to the CNO bi-cycle, the first effective reaction sequence at low temperature ($T \gtrsim 10.2 \times 10^6$ K) is the CN cycle, ${}^{12}\text{C}(p,\gamma){}^{13}\text{N}(e^+\nu){}^{13}\text{C}(p,\gamma){}^{14}\text{N}(p,\gamma){}^{15}\text{O}(e^+\nu){}^{15}\text{N}(p,\alpha){}^{12}\text{C}$. The CN cycle starts by depleting ${}^{12}\text{C}$ and producing ${}^{13}\text{C}$, which is then converted predominantly into ${}^{14}\text{N}$; the initial abundance of ${}^{15}\text{N}$ is also depleted. The steady state abundances of the secondary nuclei ${}^{13}\text{C}$ and ${}^{15}\text{N}$ are a function of temperature, such that there is a peak of ${}^{13}\text{C}$ and a valley of ${}^{15}\text{N}$ abundances and an equilibrium ratio of ${}^{15}\text{N}/{}^{14}\text{N}$ (horizontal sections of ${}^{14}\text{N}$ and ${}^{15}\text{N}$ curves).

Further inward where the temperatures are higher ($T \gtrsim 13.2 \times 10^6$ K), the ON cycle becomes effective, resulting in the production of ${}^{17}\text{O}$ and the depletion of ${}^{16}\text{O}$ and ${}^{18}\text{O}$ through ${}^{16}\text{O}(p,\gamma){}^{17}\text{F}(e^+\nu){}^{17}\text{O}$ and ${}^{18}\text{O}(p,\alpha){}^{15}\text{N}$ reactions, respectively. Approaching the previously convective core, the abundances of ${}^{12}\text{C}$, ${}^{13}\text{C}$, ${}^{17}\text{O}$, and ${}^{18}\text{O}$ increase, as does that of ${}^{23}\text{Na}$, indicating the action of the NeNa cycle. At these high temperatures ($T \gtrsim 15 \times 10^6$ K), the ${}^{22}\text{Ne}(p,\gamma){}^{23}\text{Na}$ reaction depletes ${}^{22}\text{Ne}$ and produces ${}^{23}\text{Na}$; the consequence of this reaction is that any surface abundance enhancement in ${}^{23}\text{Na}$ should be accompanied by the concomitant reduction in ${}^{22}\text{Ne}$ by approximately the same amount by number.

As noticed by El Eid (1994), inside the H convective core the CNO bi-cycle reaches an equilibrium state, and all O isotopes and ${}^{19}\text{F}$ are depleted. On the contrary, ${}^{14}\text{N}$ and ${}^4\text{He}$ are strongly produced together, accompanied by the enhancements in ${}^{12}\text{C}$ and ${}^{13}\text{C}$. In Figure 3, we show the ratio of the surface abundance before and after the first dredge-up.

Enhancements of surface abundances, ranked from the largest to the smallest, are ^{17}O , ^3He , ^{13}C , ^{14}N , ^{23}Na , and ^4He . Reductions of surface abundances, ranked from the largest to the smallest, are ^7Li , ^{10}B , ^{15}N , ^{12}C , ^{18}O , ^{22}Ne , ^{16}O , and ^{19}F . The ranking shows the relative degree of sensitivity required for dwarf and giant observations to detect the dredge-up process. Fig.3

3. HIGH-RESOLUTION SPECTROSCOPY: ANALYSIS & ABUNDANCES

3.1. The Spectra

High-resolution, high signal-to-noise (S/N) ratio spectra of our Hyades sample were obtained with the Harlan J. Smith 2.7-m telescope and the “2dcoude” cross-dispersed echelle spectrometer at the McDonald Observatory in 2004 October. The instrument configuration and spectra have been described previously in Schuler et al. (2006b). The nominal spectral resolution of our data is $R = \lambda/\Delta\lambda \approx 60,000$ (~ 2.1 pixels), with a typical S/N ratio of 150-200 for the dwarfs and 400-600 for the giants. Reductions of the spectra followed standard routines for bias subtraction, flat fielding, scattered light removal, order extraction, and wavelength calibration using the IRAF⁶ package.

Additional spectra of the Hyades giants were obtained with the Harlan J. Smith 2.7-m telescope and the 2dcoude cross-dispersed echelle spectrometer on 2008 March 18. The instrument configuration included the cs23 setting, E2 echelle grating, TK3 detector with 24 μm pixels, and a 1×1 pixel binning, resulting in a nominal resolving power of $R = 60,000$. This configuration matches exactly that from our 2004 October observations except for the echelle grating position, which was set in the more recent observations to maximize throughput in the 8727 Å [C I] region. Two 240 s integrations were taken of each γ , δ , and ϵ Tau, resulting in S/N ratios of 365, 495, and 590, respectively, in the $\lambda 8727$ region.

3.2. Stellar Parameters

The stars used for the current analysis are a subset of our larger Hyades sample for which we have high-S/N, high-resolution spectra. Stellar parameters have been derived in a consistent manner for our entire Hyades dwarf sample using published photometry for T_{eff} , the Y^2 isochrones (Yi et al. 2003) for $\log g$, and the empirical relation of Allende Prieto et al.

⁶IRAF is distributed by the National Optical Astronomy Observatory, which is operated by the Association of Universities for Research in Astronomy, Inc., under cooperative agreement with the National Science Foundation.

(2004) for microturbulent velocity (ξ). For the giants, the stellar parameters have been collated from the literature. The derivation and adoption of the stellar parameters are described in Schuler et al. (2006a,b), where a discussion of the related uncertainties can also be found. The stellar parameters of the current sample are given in Table 1. The adopted uncertainties in the stellar parameters are provided in the footnotes of Table 1; these uncertainties are the uncertainties in the absolute stellar parameters and are most appropriate for estimating the uncertainties in the derived dwarf and giant abundances. We note that the relative parameter uncertainties between the dwarfs themselves or between the giants themselves are likely smaller.

Tab.1

3.3. CNO Abundances

The chemical abundances presented herein have been derived by means of a local thermodynamic equilibrium (LTE) analysis using an updated version of MOOG, the LTE line analysis and spectrum synthesis software package (Sneden 1973; C. Sneden 2004, private communication). Model atmospheres used in the analyses were interpolated from Kurucz ATLAS9 grids generated with the convective overshoot approximation and are the same as those used in our previous Hyades studies (Schuler et al. 2006a,b). The method and atomic parameters used to derive the CNO abundances are described below.

3.3.1. Carbon

Multiple features have been used to derive the C abundances of the Hyades stars in our sample. The primary features used for this purpose are two lines of the C₂ Swan system located at 5086.3 and 5135.6 Å, although reliable measurements could only be made of the latter in the spectra of the giants. The C₂ features are blends of multiple components of the C₂ system, and therefore the abundances were derived using the spectrum synthesis method (Figure 4). The linelists for these features have been constructed using atomic data from the Vienna Atomic Line Database (VALD; Piskunov et al. 1995; Ryabchikova et al. 1997; Kupka et al. 1999, 2000) and C₂ molecular data from Lambert & Ries (1981). The transition probabilities ($\log gf$) of the C₂ and other features have been altered slightly from those given by Lambert & Reis in order to fit the $\lambda 5086$ and $\lambda 5135$ C₂ features in the Kurucz solar atlas assuming a solar C abundance of $A_{\odot}(\text{C}) = \log N_{\odot}(\text{C}) = 8.39$ (Asplund et al. 2005a).

Fig.4

Carbon abundances of the giants have also been derived using spectral synthesis of the forbidden [C I] line at 8727.13 Å. The $\lambda 8727$ [C I] line arises from an electric quadrupole

($D_2^1 - S_0^1$) transition that is strongly coupled through collisions to the C I ground state, which is populated according to Boltzmann statistics. Its strong collisional coupling to the ground state ensures that the [C I] transition also obeys Boltzmann statistics and that the $\lambda 8727$ line forms in LTE (Stürenburg & Holweger 1990). Temperature inhomogeneities due to photospheric granulation, the so-called 3D effects, are also not expected to greatly affect this line; 3D corrections for the Sun and other solar-type stars have been calculated to be ≤ 0.05 dex (Asplund 2005). For solar-metallicity giants, the correction is of similar magnitude but positive (M. Asplund, private communication). Thus, the $\lambda 8727$ [C I] line is expected to be an accurate abundance indicator for the Hyades giants. We adopt the transition probability ($\log gf = -8.136$) for this line from Allende Prieto et al. (2002), and the linelist of the surrounding features has been constructed using atomic data from VALD and CN molecular data from Gustafsson et al. (1999). As first identified by Lambert & Swings (1967), the $\lambda 8727$ C I feature is blended with a weak Fe I line at 8727.10 \AA . This Fe I line has been determined to contribute negligibly to the [C I] line strength in the solar spectrum (e.g., Lambert & Swings 1967; Gustafsson et al. 1999; Allende Prieto et al. 2002), but Bensby & Feltzing (2006) found that the Fe I line contributes more significantly to the $\lambda 8727$ feature in the spectra of stars with $T_{\text{eff}} < 5700 \text{ K}$ and those at high [Fe/H]. The Hyades giants ($T_{\text{eff}} \sim 4940 \text{ K}$, [Fe/H] = +0.13) meet both of these criteria, and thus we have included the Fe I line in our linelist. The synthetic fit to the [C I] line in the spectrum of γ Tau is shown in Figure 5 as an example of our results.

Fig.5

In addition to the forbidden [C I] and the C₂ Swan lines, we have analyzed ten CH molecular features in the wavelength interval of $4323 - 4327 \text{ \AA}$ in the spectrum of γ Tau. Abundances were derived by fitting a synthetic spectrum to each individual line so that ten separate abundance estimates were obtained. Similar to the procedure used for C₂, the linelist for the 4325 \AA region has been calibrated by fitting the Kurucz solar atlas assuming a solar C abundance of $A_{\odot}(\text{C}) = 8.39$.

The C abundances derived from the various features described above are given in Table 1. The mean abundance of the three dwarfs is $A(\text{C}) = 8.54 \pm 0.03$ (uncertainty in the mean: $\sigma_{\mu} = \sigma_{s.d.}/\sqrt{N-1}$), corresponding to a relative abundance of [C/H] = +0.15 when adopting the solar abundance of $A_{\odot}(\text{C}) = 8.39$. The fits to the C₂ Swan lines in the dwarf spectra are only mildly sensitive to the adopted T_{eff} and $\log g$ (Table 2), and we estimate the per star uncertainty due to fitting synthetic spectra to the observed blended features is ± 0.05 dex. The typical total per star uncertainty in the derived dwarf C abundances, which is obtained by adding in quadrature the individual uncertainties due to the adopted parameters and synthetic fits, is ± 0.07 dex. Inasmuch as the standard deviation about the mean is an empirical measure of actual scatter introduced by measurement and parameter uncertainties, the slight difference in the standard deviation about the mean dwarf abundance ($\sigma_{s.d.} = 0.05$)

and our estimated total per star uncertainty (± 0.07 dex) suggests that, if anything, we slightly overestimate the expected uncertainties in the *relative* dwarf parameters based upon the adopted parameter uncertainties listed in Table 1.

Tab.2

Our mean dwarf abundance of $[C/H] = +0.15$ is consistent with previously derived values, which range from $[C/H] = +0.02$ to $[C/H] = +0.18$ (Tomkin & Lambert 1978; Friel & Boesgaard 1990; Varenne & Monier 1999; Schuler et al. 2006a). All of the previously derived C abundances for Hyades dwarfs are from analyses of high-excitation C I lines; these lines are known to be sensitive to non-LTE (NLTE) effects in solar-type stars (Asplund 2005) and potentially over-excitation effects in late-G and K dwarfs (Schuler et al. 2004). The C₂ lines, which arise from electronic transitions, are not expected to be influenced by NLTE effects in solar-type stars (Asplund et al. 2005b), and the abundances of the Hyades dwarfs presented here should need no NLTE corrections.

The C abundances of the giants, derived from the three different C spectral features, are in excellent agreement and have a mean value of $A(C) = 8.17 \pm 0.01$ (uncertainty in the mean) or $[C/H] = -0.22$. The shape of the $\lambda 5135$ C₂ feature is much less affected by blends in the spectra of the giants (Figure 4), and the uncertainty in the synthetic fit is lower than that for the dwarfs and is in fact negligible relative to the errors due to the adopted T_{eff} . The typical per star uncertainty in the C₂-based abundances of the giants, dominated by uncertainties in the parameters, is ± 0.09 dex. Similar to C₂, total per star uncertainties in the [C I]-based abundances are dominated by uncertainties in T_{eff} and $\log g$ and have a typical value of ± 0.11 dex. The expected standard deviation about the mean giant C abundance is thus ~ 0.10 dex, significantly larger than the observed value of 0.03 dex; it could be the case that the inferred uncertainty in the observed mean abundance is a systematically low fluctuation from the expected uncertainty in the mean. Also, the difference in the observed and expected standard deviations about the mean could suggest that the uncertainties in the giants' *relative* parameters, particularly T_{eff} , are significantly smaller than the uncertainties we have adopted (Table 1).

The concordance in the abundances derived from the various C features for each giant is not unspectacular given the potential issues involved with deriving abundances of evolved stars from the set of spectral lines presented here. The [C I] feature is blended with a Fe I line that may be problematic in the spectra of metal-rich giants, as described above. The molecular features may also suffer from unidentified or inaccurately modeled blends in the spectra of evolved stars, as well as possibly being influenced by 3D effects due to their acute temperature sensitivity. The consistency of the abundances suggests that neither blending features, NLTE effects, nor 3D effects are a concern for these atomic and molecular lines in the Hyades giants. Our derived mean abundance is in excellent agreement with that

of Lambert & Ries (1981), who found a mean abundance of $[C/H] = -0.20$ ($\sigma_\mu = 0.01$) with typical uncertainties of ± 0.15 dex, and with the more recent work of Mishenina et al. (2006). In the latter study, the authors derived the abundances of 177 local field clump giants, including the three Hyades giants included in our study plus the fourth giant in the cluster, θ^1 Tau. These authors find for the Hyades giants a mean abundance of $[C/H] = -0.23$ ($\sigma_\mu = 0.03$), with a typical uncertainty of ± 0.20 dex.

3.3.2. Nitrogen

Adopting the mean C abundances presented above, we use spectral synthesis to derive N abundances of HIP 14976, HIP 21099, and the three giants by fitting three CN lines at 6703.98, 6706.72, and 6707.53 Å in the $\lambda 6707.8$ Li I region of our high-resolution McDonald spectra. The CN features are too weak, given our resolution and S/N, in the spectrum of the warmer dwarf HIP 19793 to obtain an accurate N abundance. We have taken the $\lambda 6707$ Li I region linelist from King et al. (1997) and updated it with new atomic data from VALD and Kurucz⁷, and refined CN line data from Mandell et al. (2004).

Slight adjustments to atomic gf values and wavelengths are made to simultaneously reproduce as well as possible the very high S/N and resolution Kurucz solar flux atlas and $R \sim 60,000$ spectra of the Hyades giants and α Cen A and B obtained by JRK with the McDonald Observatory 2.1-m Cassegrain echelle and the University of Hawai'i 2.2-m coude spectrograph, respectively, as part of other programs. Adjustments to the CN gf values from Mandell et al. (2004) are made by forcing agreement to the solar flux atlas alone. The solar-based CN line calibrations assume the input solar C and O abundances given in previous and next subsection, respectively and the solar N abundance of Asplund et al. (2005a, $A_\odot(N) = 7.78$).

The linelist is also used to derive Li abundances in the dwarfs and giants from the $\lambda 6707.8$ Li I resonance feature. The Li determinations were made after C and N abundances are determined for each star as described above (we adopt the mean N abundance of HIP 14976 and HIP 21099 for HIP 19793) so that these can be used as inputs to the Li synthesis. We assume no ^6Li content in any of our Hyades stars; the same assumption is made in the solar and α Cen syntheses used for linelist calibration. LTE Li abundances are presented in Table 1. Uncertainties in these values are dominated by those in the profile fitting and the adopted T_{eff} values, and are ± 0.05 and ± 0.07 dex for the dwarfs and giants, respectively.

⁷See <http://kurucz.harvard.edu>

The dwarf N abundances are in good agreement and have a mean value of $A(\text{N}) = 7.58 \pm 0.06$ (uncertainty in the mean) and a mean relative abundance of $[\text{N}/\text{H}] = -0.21$ when adopting the solar abundance of $A_{\odot}(\text{N}) = 7.78$. Nitrogen abundances of Hyades dwarfs in the existing literature are scant, having been reported by only two previous studies. Tomkin & Lambert (1978) derived N abundances of two Hyades F dwarfs from near-IR high-excitation N I lines and found a mean abundance of $A(\text{N}) = 8.05$ ($\sigma_{s.d.} = 0.05$) with a total uncertainty for each star of ± 0.2 dex. Adopting the solar abundance $A_{\odot}(\text{N}) = 7.99$ of Lambert (1978), who used the same N I lines, among others, and the same atomic parameters as Tomkin & Lambert (1978), the authors report a relative abundance of $[\text{N}/\text{H}] = +0.06$. The other study is that of Takeda et al. (1998), who derived a mean abundance of $A(\text{N}) = 8.34$ ($\sigma_{s.d.} = 0.12$) for nine Hyades F dwarfs from near-IR high-excitation N I lines with typical uncertainties in each measurement of 0.2 – 0.3 dex. These authors adopted a solar of $A_{\odot}(\text{N}) = 8.05$ (Anders & Grevesse 1989), giving a relative abundance of $[\text{N}/\text{H}] = +0.29$ for the Hyades dwarfs.

It is seen that the three separate estimates of the Hyades dwarf N abundance are divergent. Takeda et al. (1998) note that their result may be spurious due to poor data quality and systematic errors in their measured EWs, and the authors do not assign a high confidence level to their derived value. As noted above, both Tomkin & Lambert (1978) and Takeda et al. (1998) analyzed high-excitation N I lines in F dwarfs which are known to be sensitive to NLTE effects (Asplund 2005). NLTE calculations for the $\lambda 8683$ N I line, a line used by both Tomkin & Lambert and Takeda et al., for 160 F, G, and K dwarfs and subgiants in the solar neighborhood have been carried out by Takeda & Honda (2005); corrections for F dwarfs are on the order of -0.15 to -0.20 dex. Applying this correction to the Tomkin & Lambert (1978) abundance, taking into account a modest NLTE correction of ≤ 0.05 dex expected for the solar N I-based abundance (Asplund 2005), reduces the difference between their value and ours from 0.27 dex to ~ 0.15 dex, bringing the two results into statistical agreement. The inferred low N abundance ($[\text{N}/\text{Fe}] \sim -0.35$) of the Hyades dwarfs is at the lower limit of the observed N abundances of metal-rich dwarfs in the field, which show some scatter around $[\text{N}/\text{Fe}] \sim 0$ (Shi et al. 2002; Israelian et al. 2004; Takeda & Honda 2005).

For the giants there is also good agreement in the derived N abundances. The mean abundance is $A(\text{N}) = 7.95 \pm 0.04$ (uncertainty in the mean), corresponding to a mean relative abundance of $[\text{N}/\text{H}] = +0.17$. Similar to the case for the dwarfs, previous determinations of Hyades giants N abundances are limited to two studies. First, Lambert & Ries (1981) derived a mean N abundance of $[\text{N}/\text{H}] = +0.29 \pm 0.04$ from an analysis of all four Hyades giants. Typical uncertainties in the individual abundances are about 0.15 dex. Second, the N abundances of γ Tau and ϵ Tau were derived by Kjaergaard et al. (1982), who found

$[N/H] = +0.03$ for the former and $[N/H] = +0.02$ for the later, with uncertainties estimated to be 0.2 – 0.3 dex. Within the combined uncertainties, the three abundance estimates are in accord. The N abundances for both the dwarfs and giants are given in Table 1.

3.3.3. Oxygen

Oxygen abundances for the Hyades dwarfs and giants have been derived in our previous studies (Schuler et al. 2006a,b); here we adopt the [O I]-based abundances from the former. Similar to the $\lambda 8727$ [C I] forbidden line, the $\lambda 6300$ [O I] line is not susceptible to NLTE effects, and corrections due to 3D effects are ≤ 0.05 dex for the Sun (Asplund et al. 2004) and ≤ 0.01 for solar-metallicity giants (Collet et al. 2007). Consequently, the [O I]-based abundances for the Hyades dwarfs and giants should be robust against NLTE and 3D effects.

The O abundances for the dwarfs and giants are given in Table 1. The dwarf mean abundance is $A(O) = 8.80 \pm 0.04$ (uncertainty in the mean), corresponding to a relative abundance of $[O/H] = +0.11$ when adopting the solar abundance ($A_{\odot}(O) = 8.69$) derived from the $\lambda 6300$ [O I] line as part of our Hyades study. The mean abundance of the stars considered herein does not differ significantly from that of the larger sample presented in Schuler et al. (2006a), who report a Hyades dwarf mean abundance of $[O/H] = +0.14 \pm 0.02$ based on the analysis of six stars. The mean abundance for the giants is $A(O) = 8.77 \pm 0.02$ (uncertainty in the mean), corresponding to a relative abundance of $[O/H] = +0.08$. The O abundances of the dwarfs and giants are in good agreement. King & Hiltgen (1996) also analyzed the $\lambda 6300$ [O I] line in high-resolution spectra of Hyades dwarfs (2) and giants (4), and they found mean abundances of $[O/H] = +0.15 \pm 0.01$ for the former and $[O/H] = -0.08 \pm 0.01$ for the latter. This 0.23 dex difference is not corroborated by the results of Schuler et al. (2006a), who were able to show that the then available $\log gf$ value adopted for the Ni I blend of the 6300 Å feature was inaccurate and mainly responsible for the giant-dwarf discrepancy reported by King & Hiltgen (1996).

4. DISCUSSION

4.1. Observations vs. Models: CNO

Qualitatively, the observed dwarf and giant CNO abundances follow the predicted chemical evolution of our stellar model (Figure 3). Relative to the dwarfs, the giants’ C is depleted, N enhanced, and O essentially unchanged. This abundance pattern is indicative of the CN cycle and first dredge-up mixing. The lack of variation in the observed O abundances further

indicates that the expanding surface convection zone did not extend deep enough to reach material processed by the ON cycle.

A more quantitative comparison verifies that the observed N and O abundances are in excellent agreement with predictions. The surface abundances of our model- in both mass fraction (X) and logarithmic form- before and after the first dredge-up are given in Table 3. The surface ^{14}N abundance is predicted to increase by a factor of 2.3 after the first dredge-up. The observed mean N abundance (Table 1) of the giants, $A(\text{N}) = 7.95$, is a factor of 2.3 higher than that of the dwarfs, $A(\text{N}) = 7.58$, in perfect concordance with the prediction. The ^{16}O mass fraction is predicted to change only slightly, by less than 3%, after the first dredge-up. This small change is not manifested in the logarithmic abundances seen in Table 3 because of a similarly small dip in the H mass fraction. Regardless, this minute difference in O abundance would be lost in observational uncertainty and is considered negligible. Our observed O abundances of the dwarfs and giants, which are statistically indistinguishable, agree with the model.

Tab.3

The consistent observational and computational results do not extend to C. Observationally, the Hyades giants have a C abundance that is factor of 2.33 (0.37 dex) lower than the dwarfs. The surface ^{12}C abundance of the model is depleted by a factor of 1.5 (0.19 dex) after the first dredge-up. The observed C abundance of the giants compared to that of the dwarfs is 0.18 dex, or about a factor of 1.5, lower than the model prediction. As a consequence, the sum of C+N+O is not constant; the abundance of the giants ($A(\text{C} + \text{N} + \text{O}) = 8.91$) is only 79% of that for the dwarfs ($A(\text{C} + \text{N} + \text{O}) = 9.01$). The model predicts that this sum should remain unchanged as a MS dwarf evolves to the RGB giant clump.

The difference in the observed and modeled ^{12}C abundances cannot be attributed to the random uncertainties in the mean observed abundances, which are $\sigma_\mu = 0.03$ and 0.01 for the dwarfs and giants, respectively; the 0.18 dex discrepancy represents a $\sim 6\sigma_\mu$ result. As discussed in §3.3.1, the observed standard deviation about the mean abundance ($\sigma_{s.d.} = 0.03$) of the giants is significantly smaller than the expected value (0.10 dex) estimated by the total per star measurement and stellar parameter uncertainties. This expected standard deviation, as well as that for the dwarfs (0.07 dex), leads to expected uncertainties in the mean abundances of $\sigma_\mu = 0.05$ and 0.04 for the dwarfs and giants, respectively. The expected uncertainty in the dwarf-giant abundance difference is then 0.064 dex, and the observed 0.18 dex discrepancy is still significant at a $\sim 3\sigma_\mu$ level.

Uncertainties in the mean (actual or expected) are a measure (empirical or theoretical) of the internal random uncertainties introduced into the analysis from the *relative* measurement and parameter (T_{eff} , $\log g$, and ξ) uncertainties. The excellent agreement among the dwarf C abundances and among the giant C abundances suggest that these random uncertainties are

very small, especially for the giants since the T_{eff} sensitivities of the C_2 and [C I] abundances are grossly similar but opposite in direction. If, however, there are *systematic errors* between the dwarf and giant parameter scales, then abundance differences significantly larger than those expected from internal random uncertainties may become manifest. This does not appear to be the case here: any systematic change in the dwarf or giant stellar parameters in an effort to account for the 0.18 dex discrepancy between the observed C abundances and model predictions eliminates existing agreements between different C abundance indicators and creates new discrepancies among the abundances of other elements. For instance, the dwarfs T_{eff} would have to be decreased by 900 K to account for the C abundance discrepancy; aside from being highly improbable, such a large T_{eff} error would mean that the derived dwarf N abundances are overestimated by 1.5 dex. A change of +270 K would be needed for the giants T_{eff} to raise their C_2 -based abundance 0.18 dex; this would, however, result in a -0.14 dex decrease in the [C I]-based abundance and create a 0.32 dex discordance in the C abundances of each giant derived from these two features. Furthermore, the change in T_{eff} would raise the giant N abundances by 0.67 dex. Similarly large (> 1 dex) changes in $\log g$ are needed to bring the observed C abundances into agreement with the model, and similar disagreements among the various elements, particularly O in this case, result.

Fitting the synthetic spectra to the observed C_2 features introduces additional error into the derived abundances of the dwarfs. This can arise from both the actual matching of the observed line shapes, which are defined by multiple blending lines (Figure 4), and uncertainties in the linelist. The latter is not expected to be a significant contributor to the error in the abundances, because the dwarfs in our sample have parameters similar to those of the Sun. The linelist may be more of an issue for the giants; however, the consistent abundances derived from the CH, C_2 , and [C I] lines suggests otherwise. As for fitting the $\lambda 5135$ feature in the giant spectra, the blending of this line is less severe than for the dwarfs, and the error due to fitting the observed spectrum is negligible compared to the uncertainties due to T_{eff} and $\log g$.

As a check of the dwarf C_2 results, the C abundance of HIP19793 was derived from the equivalent widths (EWs) of two C I lines. C I lines in the spectra of solar-type dwarfs result from high-excitation transitions, and to one degree or another, all form out of LTE (Asplund 2005). The magnitude of the NLTE corrections for these lines is dependent on T_{eff} , $\log g$, [Fe/H], and [C/Fe], and for the Sun, the corrections range from -0.03 to -0.25 dex (LTE analyses overestimate the abundances), depending on the specific line in question (Asplund et al. 2005b; Fabbian et al. 2006). Because of uncertainty associated with NLTE calculations, C I lines were not used to determine the C abundances of the dwarfs and giants. However, NLTE corrections similar to those for the Sun are expected for HIP 19793 because of the similarities in their stellar parameters ⁸. The *relative* [C/H] abundance of HIP 19793

as derived from high-excitation C I lines should be a reliable indicator of its C content. The measured EWs of the two C I lines analyzed and the resulting abundances are provided in Table 4. Atomic data for these transitions were taken from Asplund et al. (2005b). The mean abundance from the C I lines is $[C/H] = +0.14 \pm 0.02$, in excellent agreement with the C₂-based values. Combining the C₂ and C I results gives a Hyades dwarf abundance of $[C/H] = +0.15 \pm 0.02$ (uncertainty in the mean).

Tab.4

The discordance between observed C abundances of clump giants and stellar evolution model predictions may not be limited to the Hyades. Mishenina et al. (2006) derived the abundances of numerous elements for a collection of giants in the Galactic disk- including the four Hyades giants, as mentioned in §3.3.1- and compared those of C, N, and Na to predictions based on STAREVOL stellar evolution models assuming $[C/Fe] = 0$ (Figures 21 – 23, therein). The giants are divided into three metallicity bins defined by $[Fe/H] < -0.15$, $-0.15 < [Fe/H] < +0.12$, and $[Fe/H] > +0.12$. For the two more metal-rich bins, the observed C abundances fall below the $[C/Fe] = 0$ evolutionary models. The evolutionary curves fit better the data if the model $[C/Fe]$ ratios are shifted by -0.15 and -0.20 dex, respectively, as Mishenina et al. show in their Figures 22 and 23; the shifts are motivated by the empirical $[C/Fe]$ vs $[Fe/H]$ trend for the giants shown in their Figure 10.

While the initial MS C abundances of the field giants cannot be recovered, the MS abundances would be expected to be higher than those of the giants, because the latter have been diluted by first dredge-up mixing of material processed by the CN cycle. Better indicators of the MS C abundances are those of current MS dwarfs at similar metallicities (e.g., Luck & Heiter 2007). C abundances of dwarfs have been the focus of numerous high-resolution spectroscopic studies focusing on Galactic chemical evolution (e.g., Gustafsson et al. 1999). There is debate as to whether or not $[C/Fe]$ ratios increase with decreasing $[Fe/H]$ (e.g., Gustafsson et al. 1999; Takeda & Honda 2005; Reddy et al. 2006) or remain flat (Bensby & Feltzing 2006) at sub-solar metallicities; however the behavior near $[Fe/H] = 0$ is consistent: $[C/Fe] \approx 0$. Down to about $[Fe/H] = -0.3$, the results remain consistent with $[C/Fe] \approx +0.10$, and at slightly super-solar metallicities, $[Fe/H] = +0.2$, C abundances range from $0 \geq [C/Fe] \geq -0.10$, depending on the study (e.g., Gustafsson et al. 1999; Bensby & Feltzing 2006). These data, when compared to the results of Mishenina et al. (2006), confirm that C abundances of dwarfs are larger than those for giants at a given metallicity. Consequently, the $[C/Fe] = -0.15$ and -0.20 stellar evolutionary models that best fit the data of the two more metal-rich bins of Mishenina et al. (2006), and indeed the $[C/Fe] = 0$ model that fits the $[Fe/H] \approx -0.15$ bin, may not be appropriate for those metallicities

⁸The following parameters have been adopted for the Sun : $T_{\text{eff}} = 5777$ K, $\log g = 4.44$, and $\xi = 1.38$

and need to be increased by 0.10 to 0.15 dex. The implication would in that case be that the stellar evolution models do not accurately predict the observed C abundances of clump giants in the Galactic disk.

A critical diagnostic of stellar evolution is the surface $^{12}\text{C}/^{13}\text{C}$ ratio. The first reaction of the CN cycle converts ^{12}C into ^{13}N which then e^+ decays to ^{13}C , and ^{13}C is subsequently converted to ^{14}N by proton capture. The $^{13}\text{C}(p,\gamma)^{14}\text{N}$ reaction lags behind the first reaction, so a decrease in ^{12}C and an accompanying increase in ^{13}C occurs. The surface $^{12}\text{C}/^{13}\text{C}$ ratio will be attenuated after the first dredge-up mixing of core material to the outer layers. Our stellar model evolves onto the MS with a surface $^{12}\text{C}/^{13}\text{C}$ ratio of about 90, the solar value, and decreases to 23.4 after the first dredge-up. This prediction matches well the observed $^{12}\text{C}/^{13}\text{C}$ ratios of the Hyades giants. Tomkin et al. (1976) analyzed ^{12}CN and ^{13}CN lines near 6300 and 8000 Å in high-resolution spectra of the four Hyades giants and found a mean value of 21.0 ($\sigma_{s.d.} = 1.8$), and Gilroy (1989) derived a mean value of 25.8 ($\sigma_{s.d.} = 1.4$) using the same ^{12}CN and ^{13}CN lines near 8000 Å.

The agreement between the observed and predicted $^{12}\text{C}/^{13}\text{C}$ ratios of the giants complicates the interpretation of the discrepant observed and modeled ^{12}C abundances. If the ^{12}C abundance of the giants has been overdepleted relative to standard stellar model predictions, the accurately predicted $^{12}\text{C}/^{13}\text{C}$ ratios suggest that the overdepletion must extend to ^{13}C , as well. It is not known what mechanism could be responsible for this overdepletion, but in light of the agreement between the observed and predicted N and O abundances, it would appear that it has to lie outside of the CNO bi-cycle. Apropos, it is not clear how the stellar evolution model can correctly reproduce the observed N, O, and $^{12}\text{C}/^{13}\text{C}$ results while concurrently failing to do the same for ^{12}C . Nonetheless, there is no compelling evidence to suggest that the highly consistent observed abundances of the dwarfs and giants are erroneous.

4.2. CAUB Model Sensitivities

We have calculated additional stellar models in an attempt to better match the observed C abundances of the Hyades dwarfs and giants while at the same time conserving the agreement with the N, O, and $^{12}\text{C}/^{13}\text{C}$ results. The model mass, metallicity, and nuclear reaction rates have all been varied to test their affect on the predicted CNO abundance evolution, but none of the changes resolve the discrepancy with the observed abundances. The empirically determined masses of the Hyades giants are well constrained to be 2.2 – 2.4 M_{\odot} (Tomkin et al. 1995; de Bruijne et al. 2001; Armstrong et al. 2006), so significant deviations from the adopted mass of our stellar model (2.5 M_{\odot}) are not expected. We thus evolved a

2.2 M_{\odot} model and found that the ^{12}C depletion factor remained unchanged at 1.5, and the ^{14}N enhancement factor was reduced from 2.3 to 2.1.

The metallicity of the Hyades open cluster has been determined by many groups, and recent determinations fall in a small range of $[\text{Fe}/\text{H}] = +0.08 - +0.16$ (Paulson et al. 2003; Taylor & Jonev 2005; Schuler et al. 2006a). Our stellar evolution model is characterized by a metallicity of $[\text{m}/\text{H}] = +0.10$ (i.e., the solar composition scaled by +0.10 dex). Our observations of Hyades dwarfs, however, indicate that the cluster has a MS composition which includes a slightly more enhanced C abundance ($[\text{C}/\text{H}] = +0.15$) and a low N abundance ($[\text{N}/\text{H}] = -0.21$). Adopting these C and N abundances while keeping the abundances of the other elements at $[\text{m}/\text{H}] = +0.10$, we have evolved a stellar model with a modified metallicity. The ^{12}C depletion factor increased marginally from 1.5 to 1.6; a more significant change occurred for the ^{14}N enhancement factor, increasing from 2.3 to 3.8.

In all of the models discussed above, the reaction rates from the NACRE compilation (Angulo et al. 1999) have been used for the CN cycle reactions (please see §2). The $^{14}\text{N}(p, \gamma)^{15}\text{O}$ reaction is the slowest of these, and as a result, the preceding $^{12}\text{C}(p, \gamma)^{13}\text{N}(e^+\nu)^{13}\text{C}$ and $^{13}\text{C}(p, \gamma)^{14}\text{N}$ reactions increase the local ^{14}N abundance at the expense of ^{12}C . A new measurement of the reaction rate for the important $^{14}\text{N}(p, \gamma)^{15}\text{O}$ reaction has been reported by Imbriani et al. (2005), who find a rate that is a factor of ~ 2 lower than that of the NACRE compilation. Incorporating the Imbriani et al. reaction rate into our stellar model produces only minor changes in the ^{12}C depletion (1.5 to 1.6) and ^{14}N enhancement (2.3 to 2.2) factors. We attempted to further increase the ^{12}C depletion factor by adopting a $^{12}\text{C}(p, \gamma)^{13}\text{N}$ rate that is a factor of 3 higher than the NACRE rate and combining that with the $^{14}\text{N}(p, \gamma)^{15}\text{O}$ rate of Imbriani et al. In this model, the ^{12}C depletion factor increased to 1.7, while the ^{14}N enhancement factor remained unchanged at 2.3. In a more extreme attempt, we used the previously mentioned increased $^{12}\text{C}(p, \gamma)^{13}\text{N}$ rate plus the $^{14}\text{N}(p, \gamma)^{15}\text{O}$ rate of Imbriani et al. decreased by a factor of 5. This model produced a ^{12}C depletion factor of 1.9 and a ^{14}N enhancement factor of 2.5. The combination of the modified rates results in a small improvement in the discrepancy between the observed and predicted level of ^{12}C depletion in the Hyades giants, but these rates are well beyond the statistical uncertainties of the experimental cross section measurements used to determine the reaction rates. Furthermore, any changes in the reaction rates affect only the CNO abundances relative to each other and cannot resolve the discrepancy between the observed dwarf and giant $A(\text{C} + \text{N} + \text{O})$ abundances.

Finally, we tested the affect of the mixing length parameter α (and thus the efficiency of the convective energy transport) on the ^{12}C and ^{14}N surface abundance evolution of the model. In all of the models discussed above, $\alpha = 2$, and new calculations with ± 1 of the

adopted value were carried out. The changes in α had essentially no effect on the ^{12}C depletion and ^{14}N enhancement factors.

4.3. The Evolution of Li: Signs of Extra Mixing?

Once our stellar model reaches the MS, most of the initial ^7Li present in the star has been destroyed as a result of convective mixing during its pre-MS evolution. At this stage, any surviving ^7Li is located near the stellar surface at an interior radius of $M_r = 2.45 - 2.50 M_\odot$ (Figure 1). For the model with simultaneous nuclear burning and mixing, the star arrives on the MS with a ^7Li surface mass fraction of 1.15×10^{-8} ; for the model in which the nuclear burning and mixing are calculated sequentially, the ^7Li surface mass fraction is 1.18×10^{-8} . After the first dredge-up and before the onset of core He burning, the total amount of ^7Li is diluted to surface mass fractions of 1.82×10^{-10} in the first model and 1.92×10^{-10} in the second model. This dilution results from mixing over the mass radii of $M_r = 0.34 - 2.50 M_\odot$. Therefore, the surface abundance of ^7Li in both models is diluted by a factor of ~ 63 as a result of the first dredge-up. During core He burning, a small amount of ^7Li is destroyed in the inner regions of the star, but the surface abundance is not affected by this.

Using our dwarfs to infer the initial Hyades Li abundance and thus test the stellar model predictions for Li evolution in our giants is complicated by the pre-MS and MS Li depletion manifest in cool Hyades dwarfs (Thorburn et al. 1993). Before circumventing this obstacle, we note that our LTE Li abundances of HIP 19793 and 21099, $A(\text{Li}) = 2.36$ and 1.20 , are in outstanding agreement with those derived by Balachandran (1995), 2.32 and 1.29 , from reanalysis of the (Thorburn et al. 1993) $\lambda 6707$ Li I line strengths using T_{eff} values identical to our own within the uncertainties. The Li abundances of HIP 14976 and HIP 21099 differ by a factor of 2, a significant result given the ± 0.05 dex per star uncertainty. This result confirms previous findings of modest but significant star-to-star Li scatter at fixed color in cool Hyades dwarfs—scatter that implicates the action of rotationally-induced main-sequence mixing (Thorburn et al. 1993).

We estimate the initial Hyades Li abundance from the maximum abundances exhibited by stars on the warm side of the F-star Li dip and at the G star Li peak in Figure 3 of Balachandran (1995). Employing the NLTE corrections (for solar metallicity) from Carlsson et al. (1994), typically -0.10 to -0.20 dex, suggests an initial Hyades Li abundance of $A(\text{Li}) \sim 3.15$. The NLTE corrections for the giants are $\sim +0.19$ dex. The NLTE Li abundance difference between γ Tau and the initial cluster value, ~ 1.9 dex, is in excellent agreement with the 1.8 dex difference predicted by our model.

However, the Hyades giants evince a spread in Li abundance that is not explained by standard stellar models. The ~ 0.35 dex difference in $A(\text{Li})$ between γ Tau and ϵ Tau is significant given the ± 0.07 dex per star uncertainty. In Figure 6 we overplot the spectra of these 2 giants, showing the marked disparity in the strength of their Li features relative to other lines in the spectra. There are several possible explanations of the Li abundance spread in the Hyades giants: differences in their evolutionary states, small mass loss ($\leq 0.02 M_{\odot}$; see Figure 1) in ϵ Tau prior to the RGB, additional mixing during the post-MS not predicted by standard stellar models (Böhm-Vitense 2004; Charbonneau & Michaud 1990) that depletes Li in ϵ Tau, or uniform additional mixing for the Hyades giants accompanied by subsequent RGB Li production in γ Tau (Pasquini et al. 2001, 2004).

Fig.6

de Bruijne et al. (2001) constructed a high-precision Hertzsprung-Russell diagram of the Hyades open cluster using Hipparcos-based secular parallaxes, and the authors showed, using a solar-metallicity 631 Myr isochrone of (Girardi et al. 2000), that the giants are of the same evolutionary state and fall squarely on the RGB clump. Furthermore, the surface gravities of the giants, both Hipparcos-based physical gravities (de Bruijne et al. 2001) and spectroscopic gravities (Smith 1999), differ by less than 0.10 dex. The mass loss hypothesis was originally proposed by Boesgaard et al. (1977), and the small amount required to explain the lower Li abundance in ϵ Tau is very tightly constrained by the steep Li profile of the stellar model shown in Figure 1.

If differential additional post-MS mixing is to explain the giant Li abundance differences, the remarkable uniformity of the CNO, Na, Mg, Al abundances suggests this mixing must be shallow. Additional valuable constraints can be provided by Be and B, which are depleted by proton capture at slightly higher temperatures than Li. Unfortunately, Boesgaard et al. (1977) were only able to derive upper limits to Be in Hyades giants, and there is no indication in the work of Duncan et al. (1998) that potential differences in B abundances in the Hyades giants were examined. New data and updated analyses of Be and B in the Hyades giants that could stringently constrain any star-to-star differences and the depth of an assumed extra-mixing mechanism to explain such differences would have great worth.

Additional theoretical work beyond the scope of that carried out here is needed to securely identify the constraints that the uniformity of CNO and Na, Mg, Al (please see below, §4.4) abundances provide on a putative Li production mechanism in γ Tau, as well as any accompanying nucleosynthetic signatures that may betray such production. If, for example, a hot bottom burning (hbb) process (believed to be responsible for Li production in some more highly evolved AGB stars; Sackmann & Boothroyd 1992) is at work, then the uniformity of the $^{13}\text{C}/^{12}\text{C}$ ratios and ^{14}N abundances in all the giants can only be understood if the ^{13}C and ^{14}N also produced in a hbb process is negligible or can be transmuted. In principle, the

latter can be accomplished via α capture, resulting in both a neutron source (from ^{13}C) and ^{19}F production (from ^{14}N). Thus, n -capture elements and ^{19}F abundances (perhaps as well as the ^{26}Al isotopic abundance) may be key diagnostics of such production. We have compared spectral regions containing several features of the light and intermediate mass s -process elements Sr, Zr, Y, and Ba. The line strengths in γ Tau and ϵ Tau are indistinguishable. Observations of HF features in the near-IR to examine F differences in the Hyades giants would be worthwhile future work.

4.4. The Abundances of Na, Mg, & Al: Signs of non-Standard Processing?

A final test of the standard stellar evolution model can be made with Na, Mg, and Al. The surface abundances of the predominant Na, Mg, and Al isotopes (^{23}Na , ^{24}Mg , and ^{27}Al) of intermediate mass MS stars may be altered if 1) the NeNa and MgAl cycles are active in the core regions, and 2) if the convection zone extends deep enough during the first dredge-up to mix to the surface material processed by these cycles. Our stellar evolution model does show signs of NeNa and to a lesser extent MgAl cycle processing in the core; however, it is only the products of the former that get mixed to the surface during the first dredge-up. The surface abundance of ^{23}Na is predicted to increase by a factor of 1.38 (0.14 dex) and the surface abundances of ^{24}Mg and ^{27}Al remain unchanged (Table 3).

We have derived Na, Mg, and Al abundances of the Hyades dwarfs and giants using an LTE EW analysis. EWs of a set of presumably unblended Na, Mg, and Al lines were determined by fitting Gaussian profiles to the spectral features using the one-dimensional spectral analysis routine SPECTRE (Fitzpatrick & Sneden 1987). Only lines that are measurable in both our dwarf and giant spectra were utilized, and our final linelist contains three lines for each Na, Mg, and Al. Uncertainties in the EWs have been estimated by comparing the results of numerous measurements of each line; these uncertainties are generally $< 5 \text{ m}\text{\AA}$. The EW measurements, along with the adopted atomic parameters from VALD, are given in Table 5.

Tab.5

The observed Na, Mg, and Al abundances are given in Table 1. The abundances are given relative to self-consistently derived solar values which negates the effects of gf value errors and mitigates NLTE and line blending effects (at least for the dwarfs). Solar EWs were measured from a high-quality sky spectrum ($S/N \approx 950$) obtained with the Harlan J. Smith 2.7-m telescope and the 2dcoude echelle spectrometer at the McDonald Observatory during our 2004 October observing run. Abundance sensitivities to the adopted parameters are given in Table 2 and result in typical uncertainties in these abundances of about ± 0.10 dex for both the dwarfs and giants.

Similar to CNO, the Na, Mg, and Al abundances show a high level of internal consistency for the dwarfs and giants. The uncertainties in the mean abundances are no more than $\sigma_\mu = 0.03$ for each element. The mean $[m/H]$ dwarf abundances range from $+0.09 - +0.11$ and relative to Fe are essentially solar. The derived abundances of the giants, on the other hand, are found to be markedly larger than those of the dwarfs; the mean abundances are $[Na/H] = +0.61 \pm 0.02$, $[Mg/H] = +0.55 \pm 0.03$, and $[Al/H] = +0.33 \pm 0.02$ (uncertainties in the means). Such large overabundances relative to the dwarfs are in stark contrast to the model predictions. As stated above, Na is the only one of these elements that is expected to have its surface abundance affected by first dredge-up mixing, and the predicted increase is only 0.14 dex. Applying this increase to the difference in the observed dwarf and giant abundances, a 0.38 dex difference remains.

No existing self-enrichment scenario can explain the large enhancements in Na, Mg, and Al abundances of the Hyades giants. The likely culprit for the highly enhanced abundances is unaccounted for NLTE effects. Unfortunately, targeted NLTE calculations for these elements in super-solar metallicity giants have not been carried out. NLTE corrections for Na abundances at $[Fe/H] = 0$ have in general been shown to be negative (Mashonkina et al. 2000; Takeda et al. 2003; Mishenina et al. 2006), in line with theoretical expectations (Asplund 2005), but positive corrections have also been suggested (Gratton et al. 1999). In light of the derived Na overabundances of the Hyades giants compared to the dwarfs, and the larger consensus in the literature, negative NLTE corrections for Na seem more likely.

From the large grid of corrections provided by Takeda et al. (2003) we can roughly estimate a NLTE Na abundance for the Hyades giants. The corrections are dependent on line strength (or metallicity) and vary from line-to-line for a given star. This effect seems to be present in our data; the strongest Na line ($\lambda 5683$; Table 5) for the giants consistently results in an abundance that is 0.10 - 0.15 dex larger than the other two Na lines (Table 6). The NLTE models of Takeda et al. (2003) are divided into 500 K and 0.1 dex in $\log g$ grid steps. The $T_{\text{eff}} = 5000$ K model with $[m/H] = 0$ is the most suitable for the Hyades giants, but with surface gravities of $\log g \approx 2.6$, they fall in between the $\log g = 3.0$ and $\log g = 2.0$ grids. We adopt the corrections of the latter, because the predicted NLTE line strengths better match our observed EWs. Applying the corrections to the individual lines of the Hyades giants (Takeda et al. models t50g20m0) and the Sun (Table 5 therein), a mean NLTE abundance $[Na/H]_{NLTE} = 0.50 \pm 0.02$ is obtained. While the line-by-line agreement in the relative abundances for each giant is improved, the overall NLTE correction amounts to only 0.11 dex, far smaller than the 0.38 dex needed to bring the observed Na abundances into agreement with the model.

Tab.6

The situation for Mg and Al is more uncertain due to the dearth of NLTE calculations

for giants, even at solar metallicities. Further complicating the matter is that theoretical considerations generally point to *positive* corrections for LTE abundances due to large photoionization cross-sections of the lower excitation levels of Mg and the ground state of Al (Asplund 2005), although actual calculations find negative corrections for at least some stars and particular transitions (Shimanskaya et al. 2000; Liu et al. 2007). Shimanskaya et al. (2000) calculated NLTE abundances for multiple Mg I lines, including two analyzed in this study, and found corrections ranging from $-0.05 - +0.02$ dex for stars with $[m/H] = 0$ and $\log g = 2.5$. Liu et al. (2007) derived Na, Mg, and Al NLTE abundances of field clump giants, and the corrections for Mg for stars with parameters similar to the Hyades giants are of the same order as those from Shimanskaya et al. The Al corrections for the Hyades-type giants are negative, with typical values of about -0.08 dex. Similar to Na, existing Mg and Al NLTE calculations fall short of the differences in the observed abundances of the Hyades dwarfs and giants.

Our stellar evolution model and observations suggest that newly synthesized Na may have been mixed from the core regions to the surface of the giants, but as Jacobson et al. (2008) point out, no firm conclusions can be made until reliable NLTE corrections are available. If NLTE effects are to account for the discrepancies between the dwarf and giant Na, Mg, and Al abundances, calculations for super-solar metallicity stars will have to produce corrections that are $0.15 - 0.40$ dex larger than those from existing solar metallicity calculations. This may not be unreasonable given the sensitivity of the NLTE corrections to line strengths. Finally, we point out that the observed overabundances of Na and Al are common characteristics of open cluster giants. Jacobson et al. (2007) has compiled from the literature Na and Al abundances of numerous open cluster giants (Figure 7 therein); the Hyades abundances fall squarely among these other data. As for Mg, many studies find near solar abundance ratios for open cluster giants (e.g., Hamdani et al. 2000; Pasquini et al. 2004), but large Mg overabundances similar to those seen in the Hyades have been observed in other open clusters (e.g., Yong et al. 2005).

5. CONCLUSIONS

We have utilized high-resolution echelle spectroscopy to derive the light element abundances of three solar-type dwarfs and three RGB clump giants in the Hyades open cluster. Treating the dwarf abundances as a proxy for the initial composition of the giants, the observed abundance patterns have been compared to a stellar evolution model calculated with the CAUB stellar evolution code. The model reproduces well the observed N and O abundances, likewise the $^{12}\text{C}/^{13}\text{C}$ ratio, but it fails to match the observed C abundances.

Whereas the model depletes the MS ^{12}C abundance by 0.19 dex, the observed mean giant abundance is 0.37 dex lower than that of the dwarfs. A similar offset between observed and modeled C abundances of giants in the Galactic disk appears also to exist (see §4.1). Random uncertainties in the mean observed abundances and uncertainties related to possible systematic errors between the dwarf and giant parameter scales have been ruled out as sources of the 0.18 dex discrepancy in the observed and predicted levels of ^{12}C depletion in the Hyades giants. Changes to the stellar model parameters fail to significantly improve the disagreement between the observations and predictions.

The observed Li abundance of the giant γ Tau is in excellent concordance with the amount of surface dilution predicted by our stellar evolution model. However, the ~ 0.35 dex spread in the Li abundances of γ Tau and ϵ Tau is not accounted for by standard stellar models. The highly consistent CNO, and Na, Mg, Al abundances of the giants place stringent constraints on any differential mixing or Li production mechanisms that may be proffered to explain the divergent abundances. Whatever the mechanism may be, it is apparent that it must be unrelated to the uniformly low ^{12}C abundances of the giants. Be and B abundances can be used to further probe possible mixing mechanisms, but unfortunately, existing data are unable to provide firm conclusions in this regard (Boesgaard et al. 1977; Duncan et al. 1998). Additional observations and theoretical efforts are needed to make further progress in understanding the Li abundances of these giants.

Na, Mg, and Al abundances of the Hyades dwarfs and giants were derived, and all three elements are greatly enhanced in the giants relative to the dwarfs. Our standard stellar evolution model predicts that the surface ^{23}Na abundance will show a modest increase (~ 0.14 dex) after the first dredge-up, but it falls far short of the observed +0.52 dex difference in the dwarf and giant abundances. The large Na, Mg, and Al overabundances of the giants cannot be explained by any known self-enrichment scenarios, and they are likely due to unaccounted for NLTE effects. Existing NLTE corrections for ^{23}Na (Takeda et al. 2003) lower the abundance of the giants by another 0.11 dex, but it too is unable to account for the large observed difference. Current NLTE calculations are limited to solar metallicities and below, so targeted calculations of super-solar metallicity stars for Na, Mg, and Al are needed.

Finally, we are left to briefly contemplate the physical implication of the disagreement between the observed C abundances of the Hyades giants and the stellar evolution model. Unlike the light element abundance patterns of low-mass metal-poor giants brighter than the RGB bump, non-canonical mixing cannot explain the overdepleted ^{12}C abundances of the Hyades giants. This leaves the possibility that additional ^{12}C , and possibly ^{13}C , has been processed during the evolution of the giants. Given the difference in the observed C+N+O

abundances of the dwarfs and giants and that the N and O abundances follow the model prediction, this depletion, if real, must have occurred via a reaction not associated with the CNO bi-cycle. At the core temperatures considered here, there is no known reaction outside of the bi-cycle that can destroy ^{12}C . Thus, our observational result may signify that an unknown nucleosynthetic process may be at work in metal-rich $2.5 M_{\odot}$ stars. Additional fine CNO abundance analyses of both MS and evolved stars in open clusters at solar metallicities and above will be helpful to further investigate this possibility and continue to test standard stellar evolution models.

S.C.S. acknowledges support provided by the NOAO Leo Goldberg Fellowship; NOAO is operated by the Association of Universities for Research Astronomy, Inc., under a cooperative agreement with the National Science Foundation. J.R.K. gratefully acknowledges support for this work by grants AST 00-86576 and AST 02-39518 to J.R.K. from the National Science Foundation and by a generous grant from the Charles Curry Foundation to Clemson University. We thank Clemson graduate student Y. Chen for her diligent work on the C_2 linelists. S.C.S. also thanks V. Smith and K. Cunha for helpful discussions.

Facilities: McD:2.7m (2dcoude)

REFERENCES

- Allende Prieto, C., Lambert, D. L., & Asplund, M. 2002, *ApJ*, 573, L137
- Allende Prieto, C., Barklem, P. S., Lambert, D. L., & Cunha, K. 2004, *A&A*, 420, 183
- Anders, E. & Grevesse, N. 1989, *Geochim. Cosmochim. Acta*, 53, 197
- Angulo, C., et al. 1999, *Nuclear Physics A*, 656, 3
- Armstrong, J. T., Mozurkewich, D., Hajian, A. R., Johnston, K. J., Thessin, R. N., Peterson, D. M., Hummel, C. A., & Gilbreath, G. C. 2006, *AJ*, 131, 2643
- Arnett, D. 1996, *Supernovae and Nucleosynthesis: An Investigation of the History of Matter, from the Big Bang to the Present*, by D. Arnett. Princeton: Princeton University Press, 1996.
- Asplund, M. 2005, *ARA&A*, 43, 481
- Asplund, M., Grevesse, N., & Sauval, A. J. 2005a, in *ASP Conf. Ser. 336, Cosmic Abundances as Records of Stellar Evolution and Nucleosynthesis*, ed. T. Barnes & F. Bash (San Francisco:ASP), 25

- Asplund, M., Grevesse, N., Sauval, A. J., Allende Prieto, C., & Blomme, R. 2005b, *A&A*, 431, 693
- Asplund, M., Grevesse, N., Sauval, A. J., Allende Prieto, C., & Kiselman, D. 2004, *A&A*, 417, 751
- Audi, G. & Wapstra, A. H. 1995, *Nuclear Physics A*, 595, 409
- Balachandran, S. 1995, *ApJ*, 446, 203
- Bensby, T. & Feltzing, S. 2006, *MNRAS*, 367, 1181
- Boesgaard, A. M., Heacox, W. D., & Conti, P. S. 1977, *ApJ*, 214, 124
- Böhm-Vitense, E. 2004, *AJ*, 128, 2435
- Brown, J. A. 1985, *ApJ*, 297, 233
- Carlsson, M., Rutten, R. J., Bruls, J. H. M. J., & Shchukina, N. G. 1994, *A&A*, 288, 860
- Charbonneau, P. & Michaud, G. 1990, *ApJ*, 352, 681
- Charbonnel, C. & Zahn, J.-P. 2007, *A&A*, 467, L15
- Clayton, D. D. 1968, New York: McGraw-Hill, 1968
- Collet, R., Asplund, M., & Trampedach, R. 2007, *A&A*, 469, 687
- de Bruijne, J. H. J., Hoogerwerf, R., & de Zeeuw, P. T. 2001, *A&A*, 367, 111
- Denissenkov, P. A., Chaboyer, B., & Li, K. 2006, *ApJ*, 641, 1087
- Duncan, D. K., Peterson, R. C., Thorburn, J. A., & Pinsonneault, M. H. 1998, *ApJ*, 499, 871
- El Eid, M. F. 1994, *A&A*, 285, 915
- El Eid, M. F., Meyer, B. S., & The, L.-S. 2004, *ApJ*, 611, 452
- Fabbian, D., Asplund, M., Carlsson, M., & Kiselman, D. 2006, *A&A*, 458, 899
- Ferguson, J. W., Alexander, D. R., Allard, F., Barman, T., Bodnarik, J. G., Hauschildt, P. H., Heffner-Wong, A., & Tamanai, A. 2005, *ApJ*, 623, 585
- Fitzpatrick, M. J., & Sneden, C. 1987, *BAAS*, 19, 1129

- Friel, E. D. & Boesgaard, A. M. 1990, *ApJ*, 351, 480
- Gilroy, K. K. 1989, *ApJ*, 347, 835
- Girardi, L., Bressan, A., Bertelli, G., & Chiosi, C. 2000, *A&AS*, 141, 371
- Gratton, R. G., Carretta, E., Eriksson, K., & Gustafsson, B. 1999, *A&A*, 350, 955
- Gratton, R. G., Sneden, C., Carretta, E., & Bragaglia, A. 2000, *A&A*, 354, 169
- Gustafsson, B., Karlsson, T., Olsson, E., Edvardsson, B., & Ryde, N. 1999, *A&A*, 342, 426
- Hamdani, S., North, P., Mowlavi, N., Raboud, D., & Mermilliod, J.-C. 2000, *A&A*, 360, 509
- Iben, I. J. 1964, *ApJ*, 140, 1631
- Imbriani, G., et al. 2005, *European Physical Journal A*, 25, 455
- Iglesias, C. A. & Rogers, F. J. 1996, *ApJ*, 464, 943
- Israelian, G., Ecuivillon, A., Rebolo, R., García-López, R., Bonifacio, P., & Molaro, P. 2004, *A&A*, 421, 649
- Jacobson, H. R., Friel, E. D., & Pilachowski, C. A. 2007, *AJ*, 134, 1216
- Jacobson, H. R., Friel, E. D., & Pilachowski, C. A. 2008, *AJ*, 135, 2341
- King, J. R., Deliyannis, C. P., Hiltgen, D. D., Stephens, A., Cunha, K., & Boesgaard, A. M. 1997, *AJ*, 113, 1871
- King, J. R. & Hiltgen, D. D. 1996, *AJ*, 112, 2650
- Kjaergaard, P., Gustafsson, B., Walker, G. A. H., & Hultqvist, L. 1982, *A&A*, 115, 145
- Kunz, R., Fey, M., Jaeger, M., Mayer, A., Hammer, J. W., Staudt, G., Harissopulos, S., & Paradellis, T. 2002, *ApJ*, 567, 643
- Kupka, F., Piskunov, N., Ryabchikova, T. A., Stempels, H. C., & Weiss, W. W. 1999, *A&AS*, 138, 119
- Kupka, F. G., Ryabchikova, T. A., Piskunov, N. E., Stempels, H. C., & Weiss, W. W. 2000, *Baltic Astronomy*, 9, 590
- Lambert, D. L. 1978, *MNRAS*, 182, 249
- Lambert, D. L. & Ries, L. M. 1977, *ApJ*, 217, 508

- Lambert, D. L. & Ries, L. M. 1981, *ApJ*, 248, 228
- Lambert, D. L. & Swings, J. P. 1967, *Sol. Phys.*, 2, 34
- Liu, Y. J., Zhao, G., Shi, J. R., Pietrzyński, G., & Gieren, W. 2007, *MNRAS*, 382, 553
- Luck, R. E. & Heiter, U. 2007, *AJ*, 133, 2464
- Mandell, A. M., Ge, J., & Murray, N. 2004, *AJ*, 127, 1147
- Mashonkina, L. I., Shimanskii, V. V., & Sakhbullin, N. A. 2000, *Astronomy Reports*, 44, 790
- Mishenina, T. V., Bienaymé, O., Gorbaneva, T. I., Charbonnel, C., Soubiran, C., Korotin, S. A., & Kovtyukh, V. V. 2006, *A&A*, 456, 1109
- Pasquini, L., Randich, S., & Pallavicini, R. 2001, *A&A*, 374, 1017
- Pasquini, L., Randich, S., Zoccali, M., Hill, V., Charbonnel, C., & Nordström, B. 2004, *A&A*, 424, 951
- Paulson, D. B., Sneden, C., & Cochran, W. D. 2003, *AJ*, 125, 3185
- Piskunov, N. E., Kupka, F., Ryabchikova, T. A., Weiss, W. W., & Jeffery, C. S. 1995, *A&AS*, 112, 525
- Rauscher, T. & Thielemann, F.-K. 2000, *Atomic Data and Nuclear Data Tables*, 75, 1
- Reddy, B. E., Lambert, D. L., & Allende Prieto, C. 2006, *MNRAS*, 367, 1329
- Ryabchikova, T. A., Piskunov, N. E., Kupka, F., & Weiss, W. W. 1997, *Baltic Astronomy*, 6, 244
- Rolfs, C. E. & Rodney, W. S. 1988, Research supported by NSF, Georgetown University, DFG, et al. Chicago, IL, University of Chicago Press, 1988, 579
- Sackmann, I.-J. & Boothroyd, A. I. 1992, *ApJ*, 392, L71
- Salaris, M., Cassisi, S., & Weiss, A. 2002, *PASP*, 114, 375
- Schuler, S. C., Hatzes, A. P., King, J. R., Kürster, M., & The, L.-S. 2006a, *AJ*, 131, 1057
- Schuler, S. C., King, J. R., Hobbs, L. M., & Pinsonneault, M. H. 2004, *ApJ*, 602, L117
- Schuler, S. C., King, J. R., Terndrup, D. M., Pinsonneault, M. H., Murray, N., & Hobbs, L. M. 2006b, *ApJ*, 636, 432

- Shetrone, M. D. 2003, *ApJ*, 585, L45
- Shi, J. R., Zhao, G., & Chen, Y. Q. 2002, *A&A*, 381, 982
- Shimanskaya, N. N., Mashonkina, L. I., & Sakhbullin, N. A. 2000, *Astronomy Reports*, 44, 530
- Smith, G. 1999, *A&A*, 350, 859
- Snedden, C. 1973, *ApJ*, 184, 839
- Stürenburg, S. & Holweger, H. 1990, *A&A*, 237, 125
- Takeda, Y. & Honda, S. 2005, *PASJ*, 57, 65
- Takeda, Y., Kawanomoto, S., Takada-Hidai, M., & Sadakane, K. 1998, *PASJ*, 50, 509
- Takeda, Y., Zhao, G., Takada-Hidai, M., Chen, Y.-Q., Saito, Y.-J., & Zhang, H.-W. 2003, *Chinese Journal of Astronomy and Astrophysics*, 3, 316
- Tautvaišienė, G., Edvardsson, B., Tuominen, I., & Ilyin, I. 2000, *A&A*, 360, 499
- Taylor, B. J. & Joner, M. D. 2005, *ApJS*, 159, 100
- The, L.-S., El Eid, M. F., & Meyer, B. S. 2000, *ApJ*, 533, 998
- The, L.-S., El Eid, M. F., & Meyer, B. S. 2007, *ApJ*, 655, 1058
- Thorburn, J. A., Hobbs, L. M., Deliyannis, C. P., & Pinsonneault, M. H. 1993, *ApJ*, 415, 150
- Timmes, F. X. & Swesty, F. D. 2000, *ApJS*, 126, 501
- Tomkin, J. & Lambert, D. L. 1978, *ApJ*, 223, 937
- Tomkin, J., Luck, R. E., & Lambert, D. L. 1976, *ApJ*, 210, 694
- Tomkin, J., Pan, X., & McCarthy, J. K. 1995, *AJ*, 109, 780
- Varenne, O. & Monier, R. 1999, *A&A*, 351, 247
- Yi, S. K., Kim, Y.-C., & Demarque, P. 2003, *ApJS*, 144, 259
- Yong, D., Carney, B. W., & Teixeira de Almeida, M. L. 2005, *AJ*, 130, 597

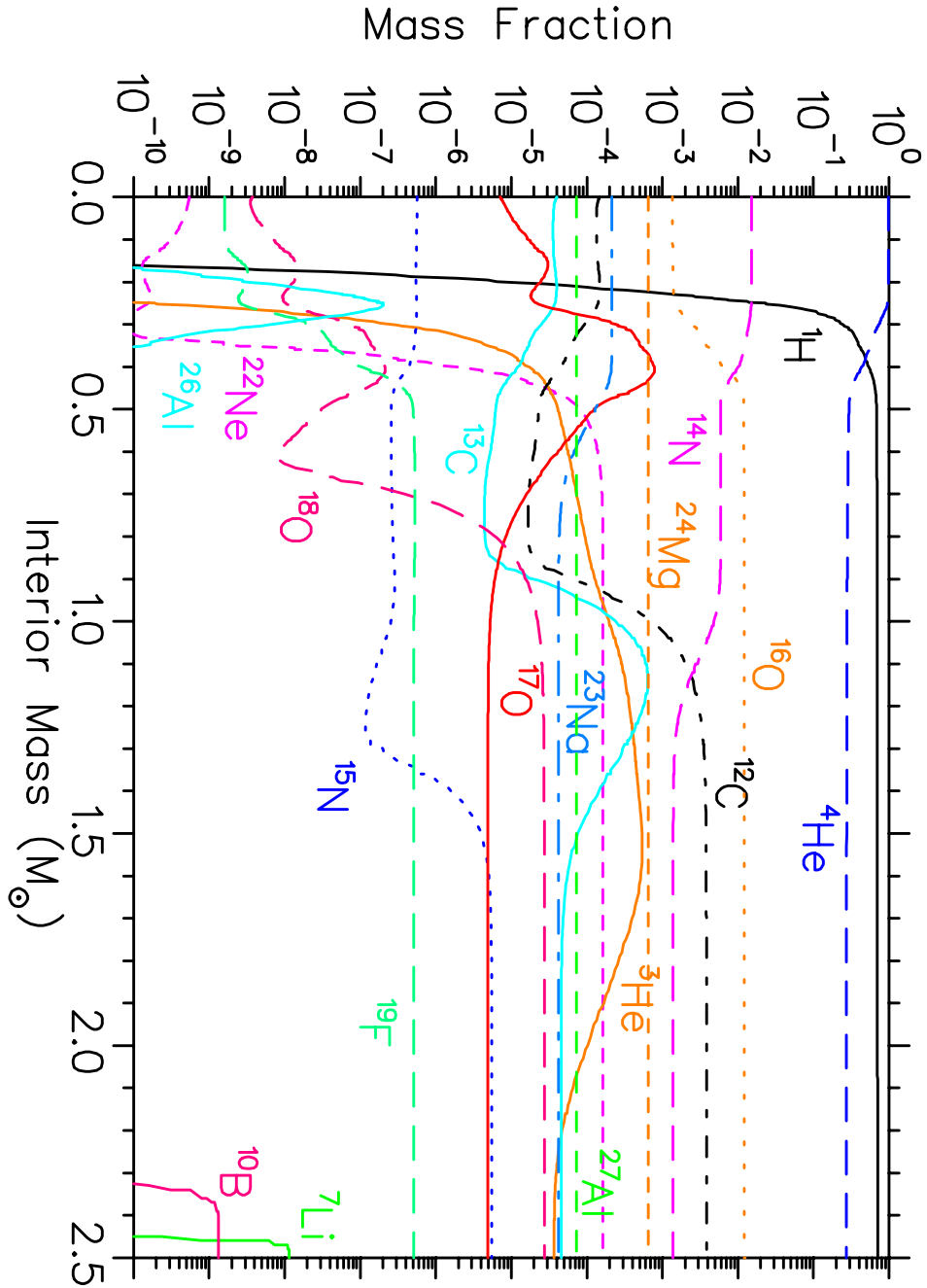


Fig. 1.— Mass fraction vs interior mass of our stellar evolution model before the first dredge-up.

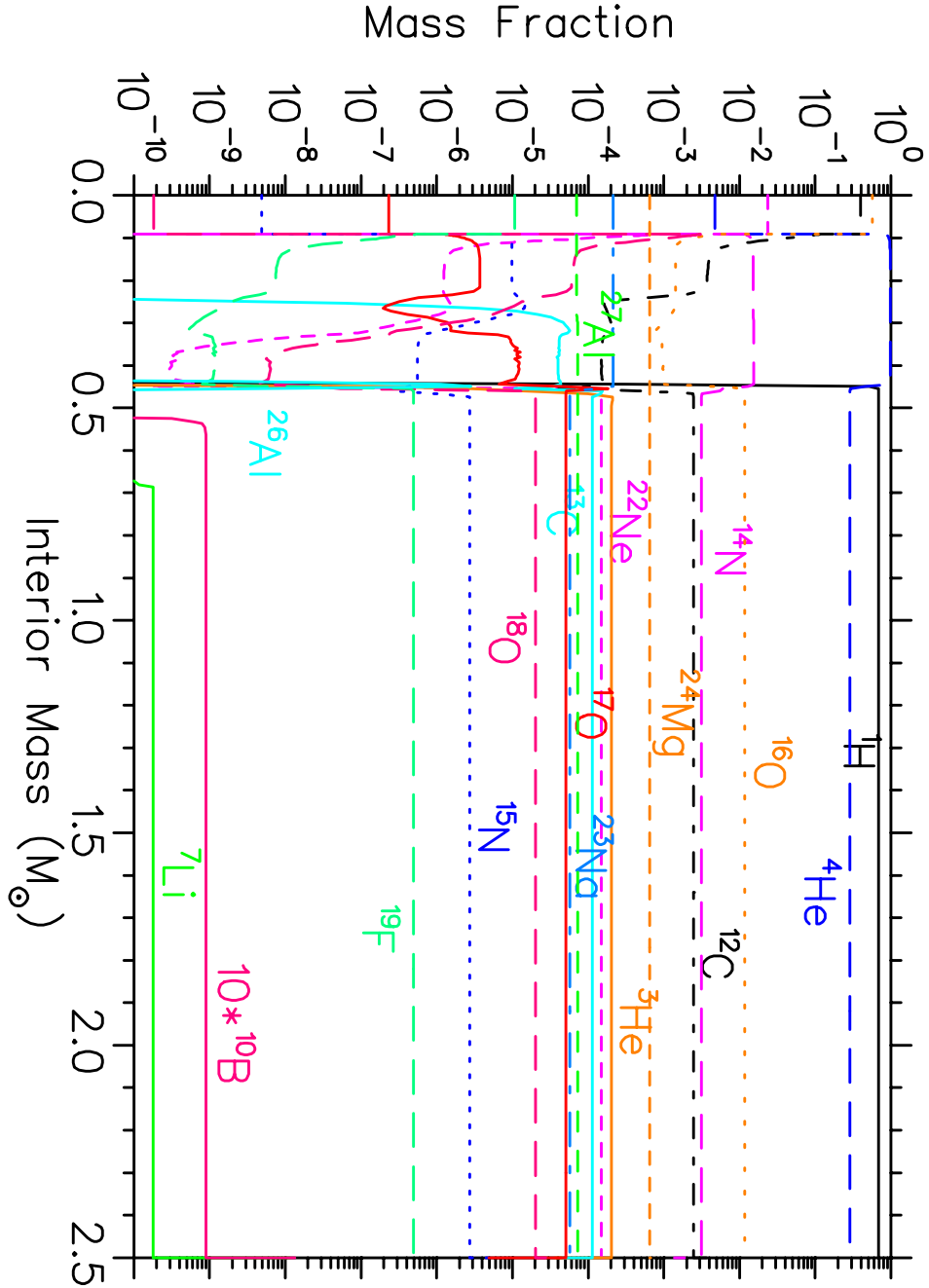


Fig. 2.— Mass fraction vs interior mass of our stellar evolution model after the first dredge-up.

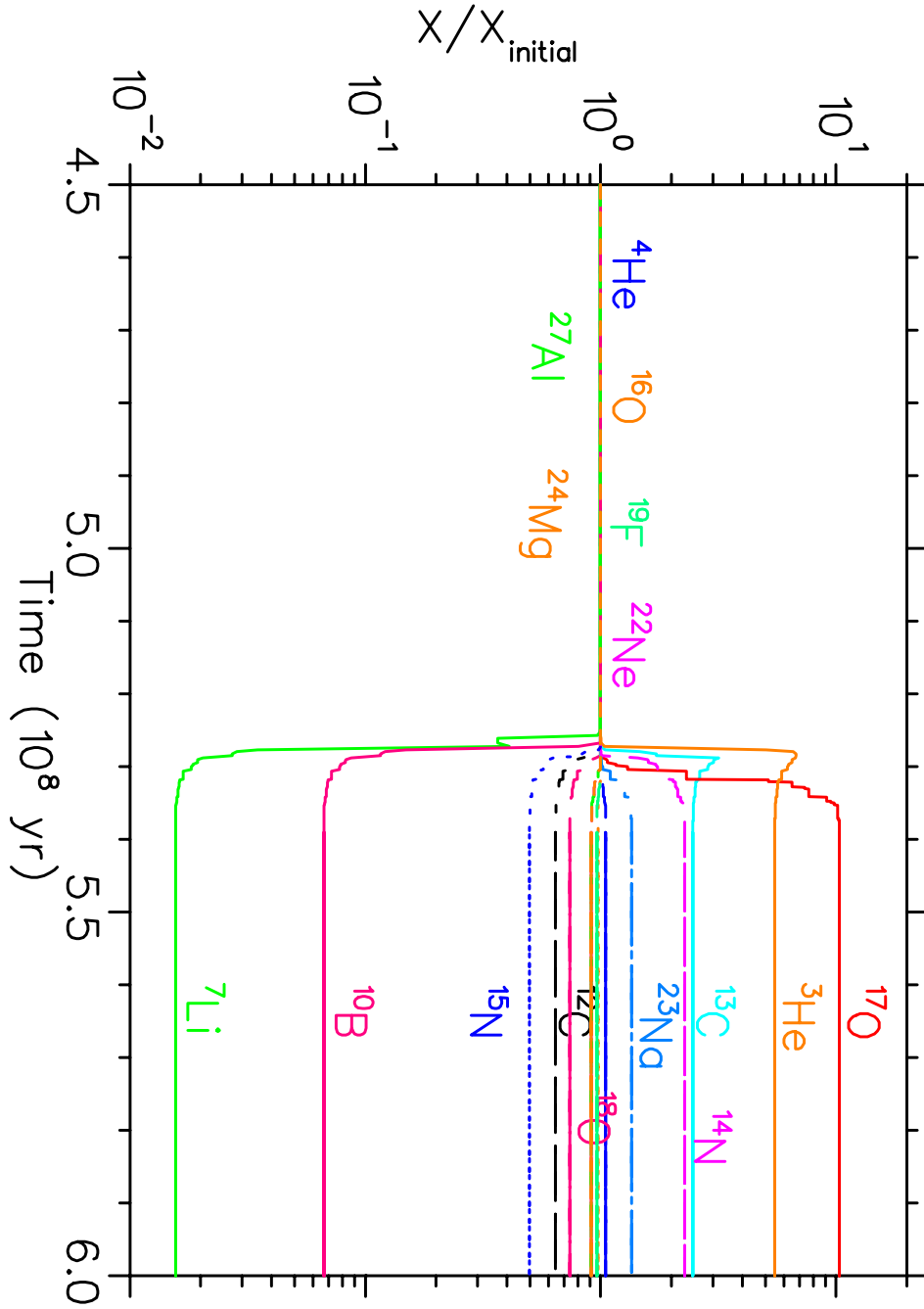


Fig. 3.— The evolution of surface abundances as a function of time.

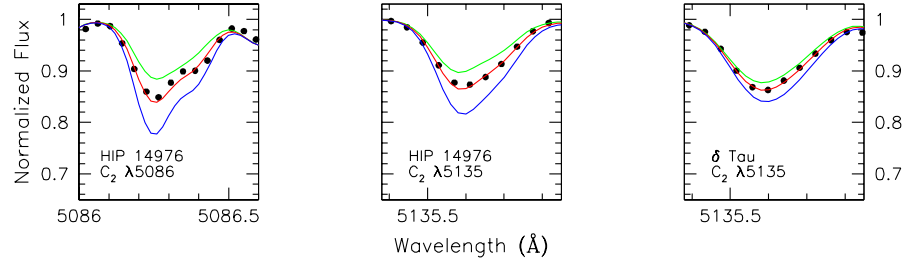


Fig. 4.— Synthetic fits to observed C₂ lines for Hyades dwarf HIP 14976 and giant δ Tau. The red lines represent the best fit abundances for each C₂ feature and correspond to $A(C) = 8.54$ and $A(C) = 8.57$ for the $\lambda 5086$ and $\lambda 5135$ features, respectively, for HIP 14976, and $A(C) = 8.15$ for δ Tau. The blue and green lines represent ± 0.10 dex of the best fit abundance.

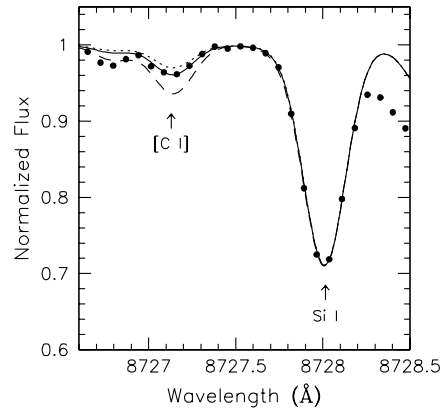


Fig. 5.— The $\lambda 8727$ spectral region of Hyades giant γ Tau. The [C I] and strong neighboring Si I lines are marked. The best fit synthetic spectrum is given by the solid line and corresponds to a C abundance of $A(\text{C}) = 8.16$. The broken lines represent syntheses with ± 0.10 dex of the best fit abundance.

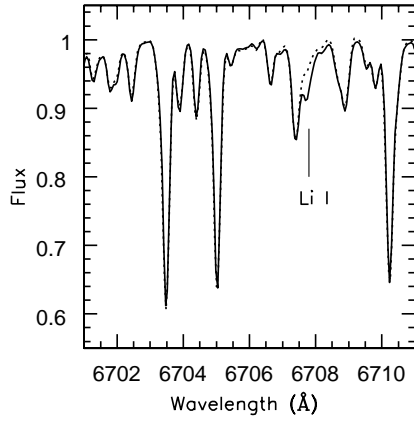


Fig. 6.— $\lambda 6707$ Li I region spectra of γ Tau (solid line) and ϵ Tau (dotted line) are overlaid. The marked difference in the strength of the Li feature relative to other lines is apparent.

Table 1. Hyades Parameters and LTE Abundances

	HIP 14976	HIP 19793	HIP 21099	γ Tau	δ Tau	ϵ Tau
Parameters:						
T_{eff} (K) ^a	5487	5722	5487	4965	4938	4911
$\log g$ (cgs) ^b	4.54	4.49	4.54	2.63	2.69	2.57
ξ (km s ⁻¹)	1.24	1.34	1.24	1.32	1.40	1.47
Abundances:						
$\log N(\text{Li}) \dots$	1.51	2.36	1.20	1.06	0.93	0.72
$\log N(\text{C}) \dots$						
CH.....	8.16
C ₂	8.57	8.48	8.56	8.18	8.15	8.13
[C I].....	8.16	8.21	8.19
$\log N(\text{N}) \dots$	7.62	...	7.53	8.01	7.95	7.90
$\log N(\text{O}) \dots$	8.74	8.82	8.84	8.74	8.80	8.76
[Na/H]....	0.06	0.13	0.07	0.63	0.58	0.61
[Mg/H]....	0.09	0.09	0.12	0.57	0.50	0.57
[Al/H].....	0.09	0.12	0.11	0.34	0.30	0.35

^aThe $1\sigma_{s.d.}$ errors in T_{eff} are 55 and 75 K for the dwarfs and giants, respectively.

^bThe $1\sigma_{s.d.}$ errors in $\log g$ are 0.10 and 0.15 dex for the dwarfs and giants, respectively.

Table 2. Abundance Sensitivities

Species	ΔT_{eff} (± 150 K)	$\Delta \log g$ (± 0.25 dex)	$\Delta \xi$ (± 0.30 km s $^{-1}$)
Dwarfs			
C ₂	± 0.03	± 0.03	0.00
N	± 0.25	∓ 0.05	0.00
O	± 0.01	± 0.11	0.00
Na	∓ 0.09	± 0.06	± 0.02
Mg	∓ 0.08	± 0.05	± 0.07
Al	∓ 0.06	± 0.05	± 0.02
Giants			
C ₂	$+0.10$ -0.18	$+0.04$ -0.01	0.00
[C I]	-0.08 $+0.12$	± 0.15	0.00
N	± 0.37	∓ 0.03	0.00
O	0.00	± 0.12	0.00
Na	∓ 0.13	± 0.05	± 0.09
Mg	∓ 0.10	± 0.04	± 0.13
Al	∓ 0.08	± 0.03	± 0.07

Table 3. Model Surface Abundances

	X	$\log N(\text{m})$	$[\text{m}/\text{H}]$
Dwarf ^a			
¹² C	3.818×10^{-3}	8.66	+0.10
¹⁴ N	1.391×10^{-3}	8.15	+0.10
¹⁶ O	1.208×10^{-2}	9.03	+0.10
²³ Na	4.204×10^{-5}	6.42	+0.10
²⁴ Mg	6.481×10^{-4}	7.58	+0.10
²⁷ Al	7.300×10^{-5}	6.59	+0.10
Giant ^b			
¹² C	2.455×10^{-3}	8.47	-0.08
¹⁴ N	3.163×10^{-3}	8.52	+0.47
¹⁶ O	1.175×10^{-2}	9.03	+0.10
²³ Na	5.693×10^{-5}	6.56	+0.24
²⁴ Mg	6.481×10^{-4}	7.59	+0.11
²⁷ Al	7.300×10^{-5}	6.59	+0.11

^aAbundances are from model #20, corresponding to a stellar age of 1.5 kyr.

^bAbundances are from model #5890, corresponding to a stellar age of 762 Myr.

Table 4. HIP 19796 C I Abundance

λ (Å)	EW_{\odot} (mÅ)	EW (mÅ)	A(C) (dex)	$[\text{C}/\text{H}]$
5380.34	21.7	26.0	8.68	+0.16
6587.61	16.2	18.6	8.64	+0.13

Table 5. Na, Mg, & Al: Spectral Line Data and Equivalent Widths

Species	λ (Å)	ξ (eV)	$\log gf$	Sun EW (mÅ)	HIP 14976 (mÅ)	HIP 19793 (mÅ)	HIP 21099 (mÅ)	γ Tau (mÅ)	δ Tau (mÅ)	ϵ Tau (mÅ)
Na I ..	5682.63	2.10	-0.70	104.0	131.0	122.8	129.8	169.7	171.3	171.3
	6154.23	2.10	-1.56	38.0	55.0	47.9	56.7	104.4	102.9	108.7
	6160.75	2.10	-1.26	58.6	76.2	69.3	78.2	120.0	120.7	125.1
Mg I ..	4571.10	0.00	-5.69	108.5	130.3	113.9	131.8	200.7	201.0	215.5
	4730.03	4.35	-2.52	71.2	93.4	83.8	94.8	122.0	122.6	129.0
	5711.09	4.35	-1.83	105.1	123.3	113.6	127.9	157.1	156.8	161.8
Al I ...	6698.67	3.14	-1.65	21.0	32.5	27.0	32.9	62.0	61.4	65.5
	7835.32	4.02	-0.65	45.0	59.2	56.0	62.8	80.8	78.7	82.8
	7836.13	4.02	-0.49	59.3	78.5	72.8	81.3	90.2	90.7	97.8

Table 6. Na, Mg, & Al: Line-by-Line Abundances

Species	λ (Å)	Sun ^a	HIP 14976	HIP 19793	HIP 21099	γ Tau	δ Tau	ϵ Tau
[Na/H]	5682.63	6.20	0.07	0.16	0.06	0.73	0.68	0.68
	6154.23	6.28	0.07	0.12	0.10	0.61	0.54	0.59
	6160.75	6.26	0.04	0.11	0.06	0.56	0.52	0.55
[Mg/H]	4571.10	7.54	0.06	0.04	0.09	0.55	0.47	0.56
	4730.03	7.87	0.14	0.15	0.16	0.58	0.53	0.61
	5711.09	7.61	0.06	0.08	0.11	0.57	0.50	0.54
[Al/H]	6698.67	6.22	0.11	0.12	0.11	0.35	0.31	0.35
	7835.32	6.41	0.07	0.12	0.11	0.36	0.30	0.33
	7836.13	6.43	0.10	0.13	0.12	0.31	0.28	0.36

^a $A(m)$ abundances are given for the Sun.